Computational Materials Science 97 (2015) 181–185

Contents lists available at ScienceDirect

Computational Materials Science

journal homepage: www.elsevier.com/locate/commatsci

Theoretical study on electronic structure, and electrical conductance at room temperature of Cu_2O–GS nanosensors and detection of H_2S gas

E. Mohammadi-Manesh [a,*], M. Vaezzadeh [a], M. Saeidi [b]

[a] Faculty of Physics, K.N. Toosi University of Technology, Tehran, Iran
[b] Department of Physics, Faculty of Basic Sciences, Shahed University, Tehran, Iran

ARTICLE INFO

Article history:
Received 10 July 2014
Received in revised form 18 October 2014
Accepted 22 October 2014

Keywords:
Graphene
Theoretical study
Hydrogen sulfide
Cu_2O
Nanosensor
Density functional theory (DFT)

ABSTRACT

In this work, adsorption of Cu_2O on a graphene which leads to production of Cu_2O–GS nanosensor and H_2S adsorption on it are computationally investigated. Adsorption energies, density of state (DOS) and room-temperature electrical conductance of Cu_2O–GS are calculated. Then a comprehensive discussion on obtained results is presented. Results show that adsorption of Cu_2O on GS leads to 2 separate configurations. DOS of both configurations is plotted and the difference between the configurations is explained. Next, adsorption energies of both configurations after H_2S adsorption are investigated. DOS of Cu_2O–GS with and without adsorbed H_2S are compared and it is shown that, according to the considerable variation of DOS after adsorption, Cu_2O–GS is an applicable nanosensor for H_2S detection. Then electrical conductance at room temperature is calculated to investigate detection capability of this nanosensor. The results illustrate that electrical conductance of the nanosensor is significantly increased by H_2S adsorption. Obtained results are in good agreement with reported experimental results.

1. Introduction

Fast and accurate detection of trace amounts of dangerous gases is an important subject in many aspects of human society, such as environmental monitoring and detection of toxic gases in industrial processes, public health, and national security. In recent years, graphene sheets (GS) are considered as an applicable material in production of chemical and biological sensors. On the other hand, cuprous oxide (Cu_2O) as a typical p-type semiconductor has attracted extensive studies on photocatalysis [1], solar cells [2], gas sensors [3], etc. due to its attractive optical and electrical properties. Rodriguez et al. [4,5], have reported that Cu_2O shows strong chemisorptions of toxic hydrogen sulfide (H_2S) gas, which predicts it has promising application in room temperature sensing for H_2S gas according to variations of conductance of the system. In the other hand, researchers [6–8], have reported that pure graphene sheet shows weak physisorption of H_2S gas and does not change its electronic properties. So, some experimental researches [9,10], have been done to investigate the adsorption of Cu_2O nanoparticles on functionalized graphene sheet (FGS) which leads to production of Cu_2O – FGS nanocomposite.

In this paper, adsorption of Cu_2O on graphene sheet which leads to production of Cu_2O–GS nanosensor is computationally investigated. Adsorption energies, density of state (DOS) of electrons and room-temperature electrical conductance of Cu_2O–GS are calculated by density functional theory (DFT) before and after adsorption of H_2S gas. The obtained results are compared to the reported experimental results to show accuracy of our computational calculations.

2. Simulation and calculation

Structure, DOS and adsorption energies of the system are simulated and calculated by QUANTUM ESPRESSO simulation package [11]. This package works based on DFT and using expansion of plane wave. After relaxation and investigation of different approximations, we used generalized gradient approximation (GGA) with Perdew–Burke–Enzerhof (PBE) functional type in which density gradient is used in addition to local density approximation to describe exchange–correlation potential. In our calculation, Rappe Rabe Kaxiras Joannopoulos (RRKJUS) method in ultrasoft pseudo potential is used to describe interaction between electron and ion in carbon, oxygen, copper and hydrogen atoms. Super cell used in the calculations is a GS with 50 carbon atoms ($4 \times 4 \times 1$ hexagonal structure). This number of carbon atoms is used to eliminate interaction between adsorbed atoms on a supercell and adsorbed

* Corresponding author.
E-mail address: emanesh@mail.kntu.ac.ir (E. Mohammadi-Manesh).

http://dx.doi.org/10.1016/j.commatsci.2014.10.043
0927-0256/

atoms on the neighbor super cell. The distance between layers is optimized to 18 Åwith considering minimization of interaction between layers for both before and after absorbance of molecules. The structure of supercell is considered as mentioned form to guarantee the uniformity of expanded supercell structure in space. The kinetic energy cutoff is optimized to 612.3 eV. We use Monkhorst pack method for *k*-points. Number of *k*-points for relaxation and self-consistent field (SCF) calculations is optimized to $6 \times 6 \times 1$ and for non self-consistent field (NSCF) calculations is optimized to $9 \times 9 \times 1$ which leads to maximum convergence in energy. Then absorbance energy and DOS for different configurations of the system are calculated by optimized parameters. The semi classical of Boltzmann transportation equation is used for calculation of electrical conductance of different configurations by Boltzmann Transport Properties (BoltzTrap) code [12]. The code uses a mesh of self-consistent band energies and is interfaced to the QUANTUM ESPRESSO simulation package. The input file for this program is results of NSCF calculations with a mesh of $30 \times 30 \times 5$ *k*-points by QUANTUM ESPRESSO. Finally components of conductance tensor are obtained.

As Fig. 1 shows, 3 different orientations for nearing Cu_2O to GS or H_2S to Cu_2O–GS are considered. Absorbance of each orientation is separately investigated in 3 positions. These 3 positions for absorbance of Cu_2O on GS include: top of carbon atom (T), perpendicular to bond of carbon–carbon (B) and top of hexagonal centre (H). So 9 possible configurations in this absorbance step are: aT, aB, aH, bT, bB, bH, cT, cB and cH. Also, according to the next section, results show that Cu_2O bonds to the GS in 2 fashions. According to the Fig. 1, we name these 2 configurations as Cu_2O–GS-1 and Cu_2O–GS-2. So 3 positions for adsorption of H_2S on Cu_2O–GS nanosensor include: top of oxygen atom in Cu_2O–GS-1 (TO_1), top of oxygen atom in Cu_2O–GS-2 (TO_2) and top of Copper atom in Cu_2O–GS-2 (TCu_2). Therefore, 9 possible configurations in this absorbance step are: aTO_1, aTO_2, $aTCu_2$, bTO_1, bTO_2, $bTCu_2$, cTO_1, cTO_2, $cTCu_2$. All mentioned calculations are done for these 18 configurations.

3. Results and discussion

3.1. Adsorption energy and DOS of Cu_2O–GS

Adsorption energy of all 9 configurations of adsorption of Cu_2O on GS are calculated by:

$$E_{adsorption} = E_{Cu_2O-GS} - (E_{GS} + E_{Cu_2O}) \quad (1)$$

The most stable configuration takes place when adsorption energy is more negative. Results show that adsorption energies in this adsorption step are −0.76 eV for aT, −0.78 eV for aH and −0.68 eV for aB. Also, the results show that these 3 adsorption states lead to a configuration which is called Cu_2O–GS-1 in Fig. 2(A). Next, adsorption energy for all bT, bH and bB are −0.85 eV which, according to Fig. 2(B), leads to a new configuration called Cu_2O–GS-2. For cT, cH and cB, the adsorption energy is positive and consequently does not lead to any absorbance.

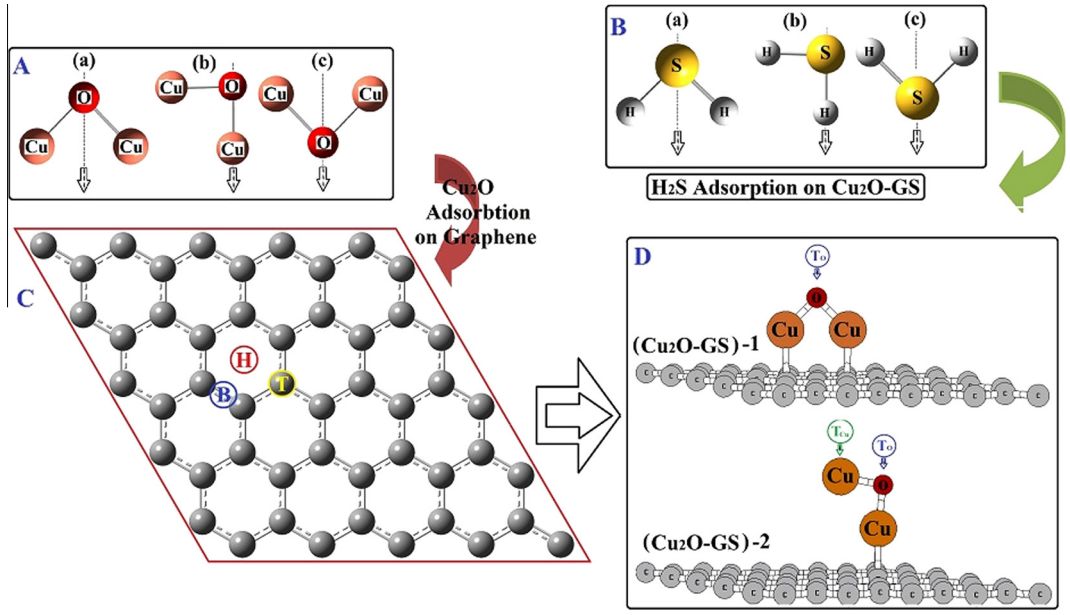

Fig. 1. (A and B) 3 different orientations for Cu_2O nearing to GS and H_2S nearing to Cu_2O–GS, (C) 3 positions for adsorption of Cu_2O on GS and (D) 3 positions for adsorption of H_2S on Cu_2O–GS nanosensor.

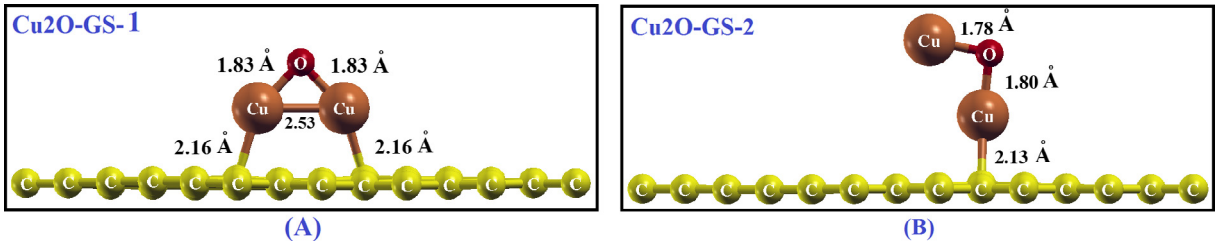

Fig. 2. Calculation results of Cu_2O adsorption on GS which show 2 possible configurations after adsorption.

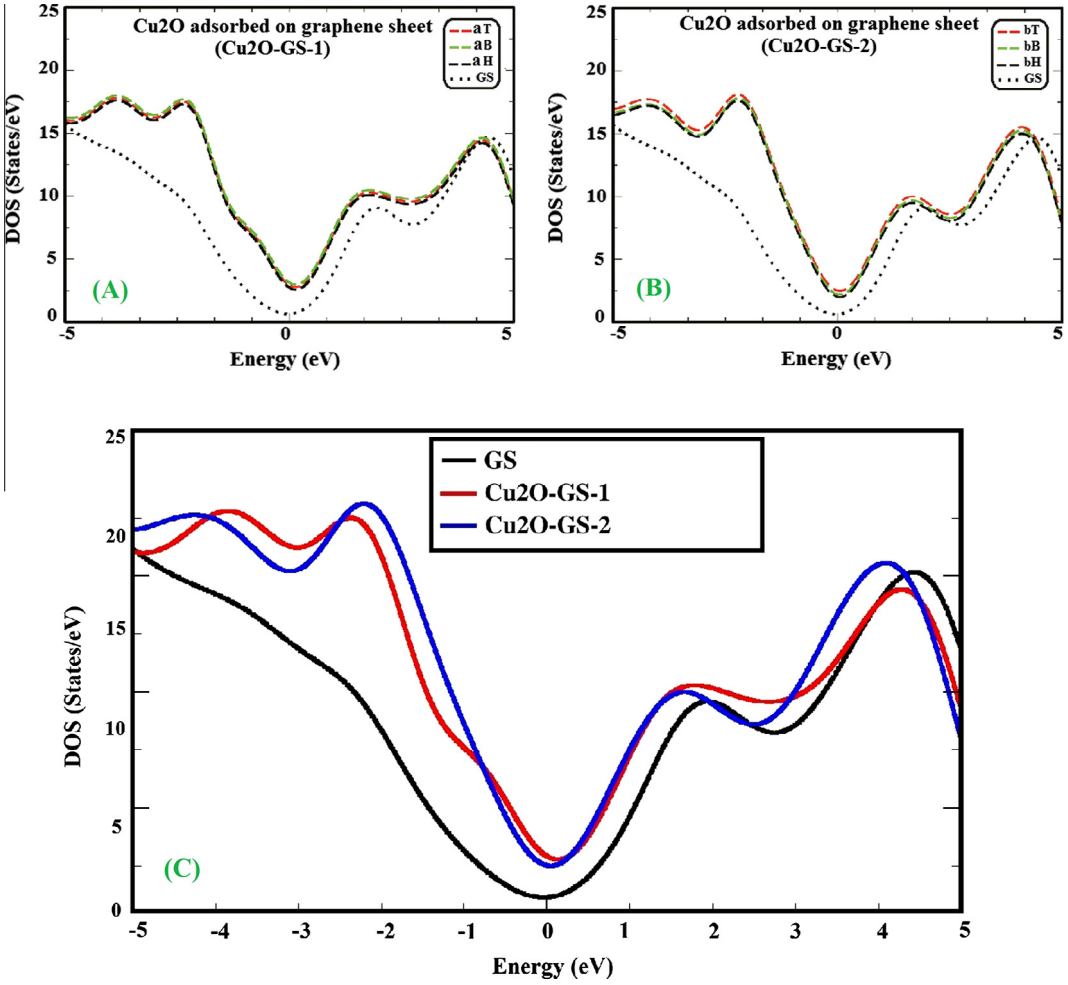

Fig. 3. DOS diagram for (A) $Cu_2O - GS - 1$ and (B) $Cu_2O - GS - 2$. (C) Comparison of DOS between GS, $Cu_2O - GS - 1$ and $Cu_2O - GS - 2$.

DOS of Cu_2O–GS-1 structure is separately calculated and plotted in Fig. 3(A) for aT, aH and aB configurations. As it is observable from adsorption energies and Fig. 3(A), DOS of each mentioned configurations is similar to other ones. It is because, in this situation, although adsorption energies are a little different but electron distribution of the system in all 3 configurations is very similar. For DOS of Cu_2O–GS-2 structure, results of DOS calculation for bT, bH and bB configurations are plotted in Fig. 3(B). It is obvious that DOS of theses 3 configurations of Cu_2O–GS-2 is identical as the same as their adsorption energies. DOS of both structures of Cu_2O–GS nanosensor is plotted in Fig. 3(C). As Fig. 3(C) shows, there is a little difference in DOS of 2 structures which is because of different orientation of nearing and bond length.

3.2. Adsorption energy and DOS of Cu_2O–GS after H_2S adsorption

In this step, adsorption energy of all 9 configurations of adsorption of H_2S on both structure of Cu_2O–GS are calculated by:

$$E_{adsorption} = E_{H_2S+(Cu_2O-GS)} - (E_{Cu_2O-GS} + E_{H_2S}) \quad (2)$$

Results show that adsorption energies in this adsorption step are −0.61 eV for aT_{Cu_2} and −0.64 eV for bT_{Cu_2} which leads to a configuration as Fig. 4 shows. But adsorption energies for cT_{Cu_2}, aTO_1, bTO_1, cTO_1, aTO_2, bTO_2 and cTO_2 are positive which do not lead to any H_2S adsorption.

In addition, DOS of Cu_2O–GS with adsorbed H_2S is calculated and plotted in Fig. 5(A). As it is observable in Fig. 5(A), DOS of Cu_2O–GS is considerably changed after adsorption which is because of variations of electron distribution by H_2S adsorption. This considerable change in DOS shows that Cu_2O–GS has capacity for application as nanosensor for H_2S detection. In next section, electrical conductance before and after H_2S adsorption is calculated to investigate detection capability of this nanosensor.

To study the changes of electronic structure in GS, and Cu_2O–GS caused by adsorption of H_2S, the net charge transfer (Q_T) between the GS and the H_2S gas, and the Cu_2O-GS and the H_2S gas were calculated using Mulliken population analysis [13]. Electron charge

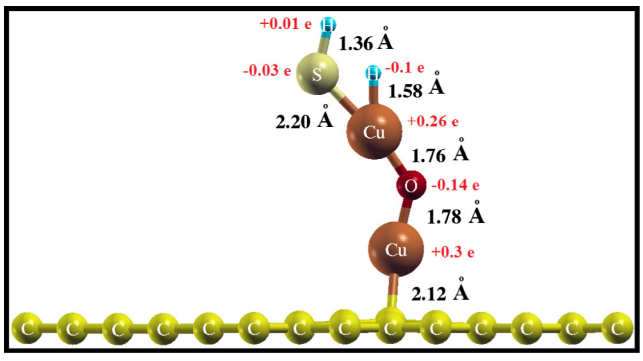

Fig. 4. Final structure of H_2S adsorption on Cu_2O–GS nanosensor for both aT_{Cu_2} and bT_{Cu_2} configurations.

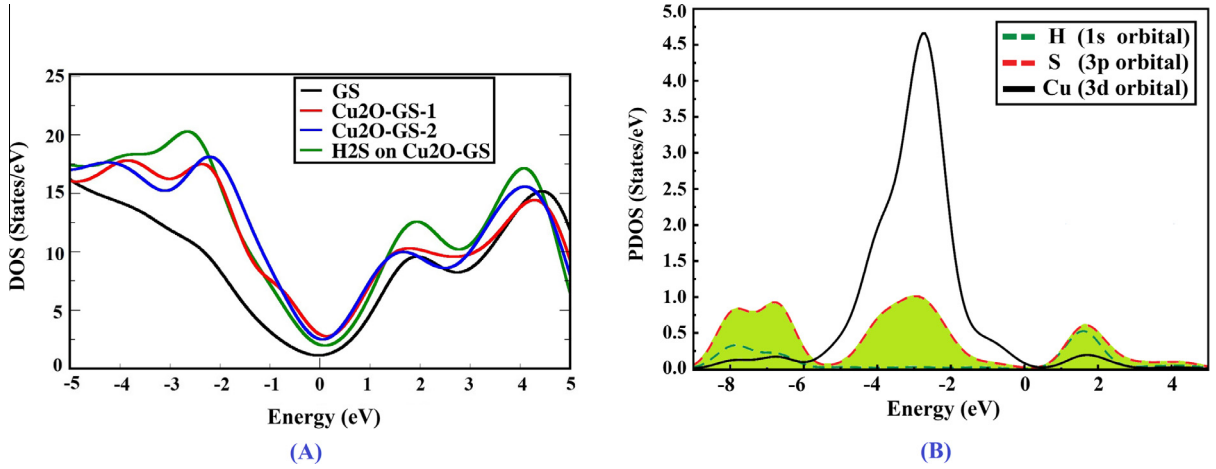

Fig. 5. (A) DOS diagrams of Cu_2O–GS-1 (red line), Cu_2O–GS-2 (blue line), Cu_2O–GS after adsorption (green line) and GS (black line). (B) The PDOS diagrams of Cu (black line), H (green dashes) and S (red dashes) of H_2S gas in the Cu_2O–GS configuration after adsorption gas. The Fermi level is set to zero. (For interpretation of the references to colour in this figure legend, the reader is referred to the web version of this article.)

transfer plays a significant role in the electronic properties and stability of an interacting system. The net charge transfer from GS to H_2S was computed to be almost 0.01 electrons (calculated identically 0.0096 electrons) that is consistent with the reported results [6]. This result confirms that the adsorption of H_2S on the GS does not change its electronic properties and shows that only a weak interaction exists between the H_2S and the GS. For Cu_2O–GS system after H_2S adsorption, the results show that 0.12 electrons are transferred from the Cu_2O to the H_2S gas (13-fold greater than for GS). Also the results show that the S atom, and the separated H carrier held 0.03, and 0.10 negative charges, respectively (Fig. 4). According to the calculation result, after adsorption of H_2S on Cu_2O–GS surface, 0.30 electrons are transferred from the Cu_2O to the GS which is in agreement with the reported experimental results [9]. To investigate the addition effect of the attached Cu_2O molecule on the H_2S adsorption, the partial density of states (PDOS) of the 3p for S atom, 1s for H atom, and 3d for Cu atom in Cu_2O-GS system with adsorbed H_2S gas were plotted, as they are shown in Fig. 5(B). The overlap between the 3p orbital of S atom and 3d orbital of Cu atom indicates that H_2S can strongly hybridize with Cu_2O.

3.3. Electrical conductance at room temperature

Next, electrical conductance of Cu_2O–GS nanosensor before and after H_2S adsorption and pure GS is calculated at room temperature and trace of conductance tensor is extracted by prefix.trace file which is an output of BoltzTrap code. Results show that conductance in *x*- and *y*-direction is identical. Also, in *z*-direction because of distance between graphene layers, conductance is very low which can be omitted. Variation of electrical conductance at room temperature versus chemical potential is plotted in Fig. 6. To plot the Fig. 6, zero point of chemical potential is assumed to be the Fermi energy level. As this Figure illustrates, after Cu_2O adsorption on GS, conductance of structure decreases in comparison with conductance of GS. When Cu_2O is adsorbed on GS, the mobility of electrons is reduced which causes conductance reduction. This observation is also reported experimentally by Zhou et al. [9], which is shown in Fig. 7.

According to the Fig. 6, electrical conductance increases after H_2S adsorption on the nanosensor. As it is mentioned in previous section, this phenomenon happens because, after H_2S adsorption on Cu_2O–GS surface, the charges are transferred from Cu_2O to GS. Also, Zhou et al. [9] reported experimentally that the reason of

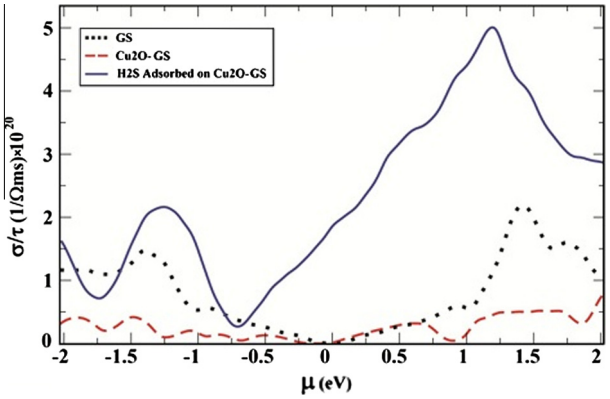

Fig. 6. Electrical conductance per decay time versus chemical potential at room temperature for GS (black dots), Cu_2O–GS (red dashes) and Cu_2O–GS after H_2S adsorption (blue line). (For interpretation of the references to colour in this figure legend, the reader is referred to the web version of this article.)

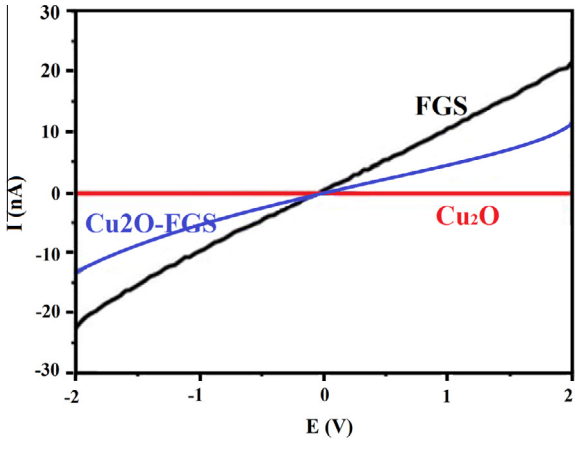

Fig. 7. Variations of current versus applied voltage to the FGS (black line), Cu_2O (red line) and Cu_2O – FGS nanosensor [6]. (For interpretation of the references to colour in this figure legend, the reader is referred to the web version of this article.)

increasing of conductance is charge transfer from Cu_2O to GS which is in agreement with our computational results. According to the measurability of conductance and considerable variations

of conductance after adsorption at room temperature, Cu_2O–GS is suggested for application as a nanosensor for H_2S detection. Also as Fig. 6 shows, increasing of the Fermi energy up to about 1.25 eV leads to increasing of conductance variance up to 2 more times; For example, an applied electric field to the nanosensor can increase its Fermi energy level [14,15]. So this nanosensor has a high sensitivity in H_2S detection.

4. Conclusion

In this paper, adsorption of Cu_2O on graphene sheet which leads to production of Cu_2O–GS nanosensor is computationally investigated and a comprehensive discussion on obtained results is presented. All calculations are done by QUANTUM ESPRESSO software and BoltzTrap code which are based on DFT and semi classical of Boltzmann transportation equation, respectively. The results show that adsorption of Cu_2O on GS leads to 2 separate configurations. Adsorption energies of both configurations after H_2S adsorption are investigated and results show that Cu_2O–GS-2 leads to H_2S adsorption. DOS of Cu_2O–GS with and without adsorbed H_2S are compared and it is shown that, according to the considerable variation of DOS after adsorption, Cu_2O–GS is an applicable nanosensor for H_2S detection. Then electrical conductance before and after H_2S adsorption is calculated at room temperature to investigate detection capability of this nanosensor. In addition, the results illustrate that electrical conductance of the nanosensor is significantly increased by H_2S adsorption. The obtained results predict that the nanosensor has promising application in room temperature sensing for H_2S gas according to variations of conductance of the system. Obtained results are compared to the reported experimental results to show accuracy of our computational calculations.

References

[1] A. Paracchino, V. Laporte, K. Sivula, M. Graetzel, E. Thimsen, Nat. Mater. 10 (2011) 456–461.
[2] L.I. Hung, C.K. Tsung, W. Huang, P. Yang, Adv. Mater. 22 (2010) 1910–1914.
[3] J.T. Zhang, J.F. Liu, Q. Peng, X. Wang, Y.D. Li, Chem. Mater. 18 (2006) 867–871.
[4] J.A. Rodriguez, S. Chaturvedi, M. Kuhn, J. Hrbek, J. Phys. Chem. B 102 (1998) 5511–5519.
[5] J.A. Rodriguez, A. Maiti, J. Phys. Chem. B 104 (2000) 3630–3638.
[6] M.D. Ganji, N. Sharifi, M. Ardjmand, M. Ghorbanzadeh Ahangari, Appl. Surface Sci. 261 (2012) 697–704.
[7] Y.H. Zhang, L.F. Han, Y.H. Xiao, D.Z. Jia, Z.H. Guo, F. Li, Computat. Mater. Sci. 69 (2013) 222–228.
[8] M.D. Ganji, N. Sharifi, M. Ghorbanzadeh Ahangari, Computat. Mater. Sci. 92 (2014) 127–134.
[9] L. Zhou, F. Shen, X. Tian, D. Wang, T. Zhang, W. Chen, RSC. Nanoscale 5 (2013) 1564–1569.
[10] C. Hou, H. Quan, Y. Duan, Q. Zhang, H. Wang, Y. Li, J. RSC. Nanoscale 5 (2013) 1227–1232.
[11] P. Giannozzi, S. Baroni, N. Bonini, M. Calandra, R. Car, C. Cavazzoni, et al., Condens. Matter. 21 (2009) 395502–395521.
[12] G.K.H. Madsen, D.J. Singh, Comput. Phys. Commun. 175 (2006) 67–71.
[13] R.S. Mulliken, J. Chem. Phys. 23 (1955) 1833–1840.
[14] A.M. Chen, First-principles Modeling of Thermoelectric Materials, Ph.D. thesis, university of Wien (2012).
[15] Y.J. Yu, Y. Zhao, S. Ryu, L.E. Brus, K.S. Kim, P. Kim, Nano Lett. 9 (2009) 3430–3434.